Secondary Structural Elements within the 3′ Untranslated Region of Mouse Hepatitis Virus Strain JHM Genomic RNA

Qi Liu, Reed F. Johnson and Julian L. Leibowitz
J. Virol. **2001, 75(24):12105. DOI: 10.1128/JVI.75.24.12105-12113.2001.**

JOURNAL OF VIROLOGY, Dec. 2001, p. 12105–12113 Vol. 75, No. 24
0022-538X/01/$04.00+0 DOI: 10.1128/JVI.75.24.12105–12113.2001

Secondary Structural Elements within the 3′ Untranslated Region of Mouse Hepatitis Virus Strain JHM Genomic RNA

QI LIU, REED F. JOHNSON, AND JULIAN L. LEIBOWITZ*

Department of Pathology and Laboratory Medicine, Texas A&M University System Health Science Center, College Station, Texas 77843-1114

Received 27 June 2001/Accepted 18 September 2001

Previously, we characterized two host protein binding elements located within the 3′-terminal 166 nucleotides of the mouse hepatitis virus (MHV) genome and assessed their functions in defective-interfering (DI) RNA replication. To determine the role of RNA secondary structures within these two host protein binding elements in viral replication, we explored the secondary structure of the 3′-terminal 166 nucleotides of the MHV strain JHM genome using limited RNase digestion assays. Our data indicate that multiple stem-loop and hairpin-loop structures exist within this region. Mutant and wild-type DIssEs were employed to test the function of secondary structure elements in DI RNA replication. Three stem structures were chosen as targets for the introduction of transversion mutations designed to destroy base pairing structures. Mutations predicted to destroy the base pairing of nucleotides 142 to 136 with nucleotides 68 to 74 exhibited a deleterious effect on DIssE replication. Destruction of base pairing between positions 96 to 99 and 116 to 113 also decreased DI RNA replication. Mutations interfering with the pairing of nucleotides 67 to 63 with nucleotides 52 to 56 had only minor effects on DIssE replication. The introduction of second complementary mutations which restored the predicted base pairing of positions 142 to 136 with 68 to 74 and nucleotides 96 to 99 with 116 to 113 largely ameliorated defects in replication ability, restoring DI RNA replication to levels comparable to that of wild-type DIssE RNA, suggesting that these secondary structures are important for efficient MHV replication. We also identified a conserved 23-nucleotide stem-loop structure involving nucleotides 142 to 132 and nucleotides 68 to 79. The upstream side of this conserved stem-loop is contained within a host protein binding element (nucleotides 166 to 129).

Coronaviruses are single-stranded, message sense, nonsegmented RNA viruses (16, 18). They are widespread pathogens infecting humans and a variety of animals (26). Mouse hepatitis virus (MHV), the most extensively studied coronavirus, possesses all of the common coronavirus characteristics (31). MHV replicates entirely in the cytoplasm (33) and causes a broad spectrum of diseases in mice (2, 17). During MHV infection, the 32-kb genomic RNA functions as an mRNA. Seven or eight different-size mRNAs are generated (18, 29, 32), which make up a 3′-coterminal nested set (15, 18). Studies of MHV mRNAs have demonstrated another unique feature. They all contain 70- to 80-nucleotide (nt) leader sequences at their 5′ termini (14, 28). The 5′ leader sequence is derived from the 5′ terminus of the genomic RNA (14).

Elucidating how mRNA is synthesized is crucial for determining MHV replication strategies. Reverse-genetic approaches to study MHV replication have been limited to date because MHV's large genome size has prevented the construction of a full-length infectious clone. Over the past decade, defective-interfering (DI) RNAs derived from MHV genomic RNA have been utilized to study the sequence and structural requirements for RNA replication with the help of wild-type virus (5, 12, 19, 22). At least 474 nt from the 5′ terminus of genomic RNA and 436 nt from the 3′ terminus as well as 57 nt from an internal region of genomic RNA are required for DI RNA replication (11). Later studies found that only the last 55 nt at the 3′ end plus a poly(A) tail are required for negative-strand RNA synthesis (20). Since 436 nt at the 3′ terminus are a necessary *cis*-acting signal for RNA replication (12, 19), it is reasonable that a much longer 3′-terminal nucleotide sequence is required for positive-strand RNA synthesis.

Our laboratory has been focusing on precisely identifying and characterizing *cis*-acting sequences at the 3′ terminus of the MHV genome that interact with host proteins and that function in MHV replication. In earlier studies we used RNase T_1 protection/gel mobility shift electrophoresis assays to identify two host protein binding elements (21, 37). One protein binding element, the 3′(+)42 element, is made up of the last 42 nt of the MHV genome upstream of the poly(A) tail, within the 55-nt minimal *cis*-acting signal for negative-strand RNA synthesis. The other maps to a 38-nt element positioned at nt 166 to 129 of the MHV strain JHM (MHV-JHM) genome (all RNAs are numbered such that position 1 represents the first nucleotide upstream of the 3′-terminal poly[A] tail). Site-directed mutagenesis coupled with DI RNA replication assays indicate that the two host protein binding elements are essential for DI RNA replication (21, 36).

Host or viral protein binding elements usually contain extensive secondary structures. It is possible that many of these secondary structural elements function in viral replication (1, 4, 35). We hypothesize that secondary structures containing the two host protein binding elements within the 3′ untranslated region (UTR) identified by our laboratory are necessary for MHV RNA replication. To determine functional roles of secondary structures of these two host protein elements, espe-

* Corresponding author. Mailing address: Department of Pathology and Laboratory Medicine, Texas A&M University System Health Science Center, 1114 TAMU, College Station, TX 77843-1114. Phone: (979) 845-7288. Fax: (979) 862-1299. E-mail: jleibowitz@tamu.edu.

TABLE 1. Primers used for primer extension, site-directed mutagenesis, and RT-PCR

Primer (application)	Sequence[a]
5530A (PCR)	CGA CTA GTG AAA GAG ATT GCA AAA TAG AG
5530B (PCR)	CGT ACG CGT TTT TTT TTT TGT GAT TCT TCC AAT TGG C
5638B (primer extension)	TTT TTT TTT TTG TGA TTC
5638C (primer extension)	TTT TTT TTT TTG TGA TTC TTC C
5665 1A (stem A1 mutation)	GAG ATT GCA AAA TAG AGA ATG T**CA CT**G AGA AGT TAG CAA GGT CCT ACG
5665 1B (stem A1 mutation)	CTC TAA CGT TTT ATC TCT TAC A**GT GA**C TCT TCA ATC GTT CCA GGA TGC
5692 A (stem A2 mutation)	GGC GCC CCC TGG GAA GAG C**AG TG**A TCA GGG TAC TAT TCC TGC
5692 B (stem A2 mutation)	CCG CGG GGG ACC CTT CTC G**TC AC**T AGT CCC ATG ATA AGG ACG
5665 3A (stem B2 mutation)	GAG AGA AGT TAG CAA GGT CCT A**GC AG**T AAC CAT AAG AAC GGC GAT AG
5665 3B (stem B2 mutation)	CTC TCT TCA ATC GTT CCA GGA T**CG TC**A TTG GTA TTC TTG CCG CTA TC
5692 C (stem B1 mutation)	CCT ACG TCT AAC CAT AAG AAC **CTG C**AT AGG CGC CCC CTG GGA AGA GC
5692 D (stem B1 mutation)	GGA TGC AGA TTG GTA TTC TTG **GAC G**TA TCC GCG GGG GAC CCT TCT CG
5665 4A (stem C mutation)	CCT GGG AAG AGC TCA CAT **GTC CC**T ACT ATT CCT GCA ATG CCC
5665 4B (stem C mutation)	GGA CCC TTC TCG AGT GTA **CAG GG**A TGA TAA GGA CGT TAC GGG
5666 (sequencing)	GTA GTG CCA GAT GGG TTA
2464 (RT and 5′ PCR)	GGC GTT GTC TAA AGA GAT TTG
1956 B (3′ PCR)	GTG ATT CTT CCA ATT GGC

[a] Boldface indicates transversion mutations.

cially the relationship between structure and viral replication, we characterized the secondary structure of the 3′-terminal 166 nt of the MHV-JHM genome. Our data showed that multiple stem-loop structures existed in this region. We identified a 23-nt conserved stem-loop structure based on enzymatic probing, phylogenetic comparison between MHV and bovine coronavirus, and computerized M*fold* prediction. Site-directed mutagenesis and DI RNA replication assays indicated that secondary structural elements play important roles in DI RNA replication.

MATERIALS AND METHODS

Virus and cells. Murine 17Cl-1 cells were grown with Dulbecco's modified Eagle medium (Life Technologies) supplemented with 10% fetal bovine serum, 4 mM glutamine, and penicillin and streptomycin, each at 50 μg/ml. Neurotropic MHV-JHM was propagated as previously described and used as a helper virus throughout this study (18).

Plasmid construction of an in vitro transcription template. To produce a transcription template for the 3′-terminal 166 nt of the MHV genome, PCR was conducted using primers listed in Table 1 to incorporate an *Spe*I site at the 5′ end and an *Mlu*I site along with 11 Ts at the 3′ end of the PCR product. The *Spe*I-*Mlu*I-digested PCR product was gel purified and ligated into plasmid LITMUS 38 (New England Biolabs) using T4 DNA ligase (Life Technologies). Colonies were screened by PCR using the primer set described above and verified by restriction digestion with enzymes *Mlu*I, *Spe*I, and *Sal*I. Selected plasmids were sequenced to confirm the presence of the entire cDNA fragment, consisting of 166 nt plus 11 Ts.

In vitro transcription and gel purification. The RNA consisting of 166 nt plus 11 A's (166 + 11A RNA) was transcribed by T7 RNA polymerase (Life Technologies) from an *Mlu*I-linearized recombinant plasmid LITMUS 38 template. In vitro transcription was conducted in accordance with the manufacturer's protocol. After 1 h of incubation at 37°C, an additional 50 U of T7 RNA polymerase was added to the reaction mixture and the mixture was incubated for another 90 min to produce maximal amounts of RNA transcripts. RNA transcripts were resolved by 7 M urea–6% polyacrylamide gel electrophoresis (PAGE). Full-length transcripts were located by UV shadowing and excised from the gel. The RNAs were eluted from the gel slices at 4°C in 0.3 M sodium acetate buffer (pH 5.2) overnight. The eluted RNAs were purified by phenol-chloroform extraction and ethanol precipitation. RNAs were quantitated by spectrophotometry and stored at −80°C.

Dephosphorylation and 5′ end labeling. Purified RNAs were dephosphorylated at their 5′ ends with shrimp alkaline phosphatase (Amersham), extracted with phenol-chloroform, and precipitated with ethanol. Dephosphorylated RNAs (5 pmol) were 5′ end labeled with [γ-^{32}P]ATP (50 μCi; ICN) by incubation with 5 U of T4 polynucleotide kinase (Life Technologies) at 37°C for 30 min. Full-length 5′-end-labeled RNAs were resolved by 7 M urea–6% PAGE and recovered from the gel as described above.

Limited RNase digestion assay. 5′-end-labeled RNAs were dissolved in 5 μl of renaturation buffer (20 mM HEPES-NaOH [pH 7.0], 200 mM NaCl, 1 mM dithiothreitol, 10 mM $MgCl_2$, and 200 μg of tRNA/μl) and incubated at 65°C for 10 min, followed by 20 min at room temperature. Digestion reactions with RNase T_1 (0.0002 U), A (0.0002 U), and CV1 (0.07 U) were performed at 0°C for 30 min. All RNases were obtained from Pharmacia Biotech. For RNase U2 (2 U), the digestion buffer contained 50 mM citric acid–sodium citrate, pH 5.0, 2 mM $MgCl_2$, and 200 μg of tRNA/μl. The digestion products were analyzed on 7 M urea–10 or 20% PAGE gels. Alkaline hydrolysis was performed at 90°C for 5 min in 50 mM $NaHCO_3$-Na_2CO_3, pH 9.0, buffer to generate an RNA ladder.

Primer extension. The primers (Table 1) were 5′ end labeled by T4 polynucleotide kinase (Life Technologies) with [γ-^{32}P]ATP (ICN) for 30 min at 37°C. The labeled primers were then resolved by 7 M urea–10% PAGE and purified. The purified full-length 166 + 11A RNAs were digested with RNase T_1 (0.0002 U), A (0.0002 U), U2 (2 U), and CV1 (0.07 U) as described above. The digested products were purified by phenol-chloroform extraction and ethanol precipitation. Digested RNAs (100 ng) were incubated with the 5′-end-labeled primer (10 ng) at 75°C for 10 min, followed by incubation at room temperature for 30 min. Fifteen microliters of RNA-primer hybrids was mixed with 10 μl of 5× reverse transcription buffer (Life Technologies), 5 μl of 100 mM dithiothreitol, 10 μl of 5 mM deoxynucleoside triphosphate mixture, 0.75 μl of RNase inhibitor (40 U/μl; Promega), and 7.25 μl of diethyl pyrocarbonate-treated H_2O. The reaction mixture was incubated at 42°C for 2 min. Four hundred units of Superscript II reverse transcriptase (200 U/μl; Life Technologies) was added, and the incubation was continued at 42°C for 50 min, followed by 70°C for 15 min. The extension products were purified by phenol-chloroform extraction and ethanol precipitation. The purified cDNA fragments were resolved by 7 M urea–10% PAGE. Sequencing ladders were generated from plasmid DE25, derived from the MHV-JHM DIssE RNA, which contains the entire 166-nt cDNA, using oligonucleotides 5638B and 5638C as the sequencing primers (Table 1). Dideoxy DNA sequencing reactions were carried out by the procedures provided with the sequencing kits (U.S. Biochemicals). Primer extension products and DE25 DNA sequence ladders were resolved by 7 M urea–10% PAGE.

Secondary structure modeling. The secondary structure prediction of 166 + 11A RNA was based on the Zuker group's algorithms, thermodynamics, and databases for RNA secondary structure (http://bioinfo.math.rpi.edu/~mfold). All modeling was accomplished using M*fold*, version 3.0.

Construction of mutant DI plasmids. To generate a plasmid to serve as a template for mutagenesis, DE25 was digested with *Spe*I and *Eag*I to liberate an 801-bp DNA fragment. The larger *Spe*I-*Eag*I fragment was treated with DNA polymerase I large (Klenow) fragment (Life Technologies) and self-ligated to yield a DE25 deletion mutant, named 5662-2. 5662-2 was mutagenized using the QuickChange site-directed mutagenesis kit (Stratagene) in accordance with the manufacturer's recommended procedures and with the primer sets listed in Table 1. Colonies were screened by DNA sequencing to confirm the presence of the introduced mutations. *Nru*I-*Xba*I fragments containing the desired mutations

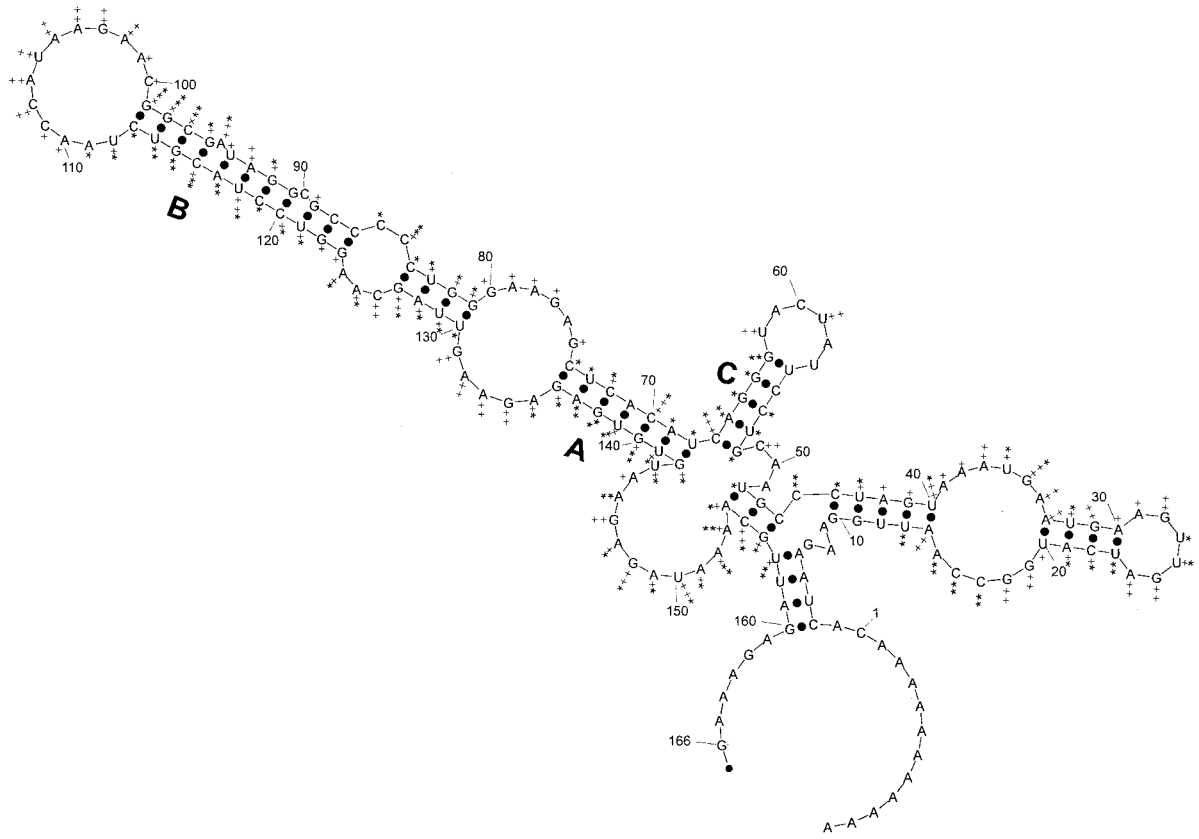

FIG. 1. Computer-predicted secondary structure model of the 3′-terminal 166 nt of MHV-JHM genomic RNA. M*fold*, version 3.0, was used to generate thermodynamically stable secondary structures, and the model which best fits the experimental data is shown. The nucleotide position was numbered such that nt 1 is immediately 5′ to the poly(A) tail. The summary of enzymatic probing data is noted at each nucleotide: ++, strongly cut by single-strand-specific enzyme; +, weakly cut by single-strand-specific enzyme; **, strongly cut by double-strand-specific enzyme; *, weakly cut by double-strand-specific enzyme, **+, strongly cut by double-strand-specific enzyme and weakly cut by single-strand-specific enzyme, ++*, strongly cut by single-strand-specific enzyme and weakly cut by double-strand-specific enzyme.

from 5662-2 were exchanged with the corresponding fragment from wild-type DE25, and the resulting plasmids were sequenced to verify the introduced mutations.

DI RNA transfection and gel electrophoresis. Wild-type and mutant DE25 DNAs were linearized by *Xba*I digestion and gel purified. The linearized plasmids were transcribed in vitro using T7 polymerase (15 U/μl; Promega) and an RNA cap structure analog (New England Biolabs) to generate mRNAs. DI RNAs were then treated with RNase-free DNase (1 U/μl; Promega) and extracted twice with phenol-chloroform and twice with chloroform. Further purification of DI RNAs was conducted using Microcon10 filters (Millipore). Purified DI RNAs were precipitated by ethanol and dissolved in diethyl pyrocarbonate-treated water. DI RNAs were transfected using Cellfectin (Life-Technologies) into 17Cl-1 cells 1 h after infection with MHV-JHM in accordance with the protocol described by Yu and Leibowitz (36). When approximately 20% of the cells had undergone cell-cell fusion (typically at 9 h postinfection), the cultures were labeled with [^{32}P]orthophosphate in the presence of actinomycin D for 2 to 3 h until syncytia involved 80% of the cells. Total RNA was extracted, and DI RNA replication was assayed by agarose gel electrophoresis as described previously (36) with the additional step that mRNA7 was used to normalize Phosphorimager data (Molecular Dynamics).

RT-PCR analysis of recombination. Isolated intracellular RNA was treated with 10 U of RNase free-DNase at 37°C for 30 min. RNA was extracted with phenol-chloroform and precipitated with ethanol. Five micrograms of RNA was assayed by PCR without a reverse transcription step to assure that no contaminating transcription template DNA was present. Primers 2464 and 1956B (Table 1) were used in the PCR. Reverse transcription-PCR (RT-PCR) for negative-strand DI RNA was performed as previously described (36). PCR products were purified using the Wizard PCR Prep kit (Promega). DNA sequencing was carried out to determine if the intended mutant sequences were maintained in the replicating DI RNA or had been replaced by wild-type sequences.

RESULTS

Secondary structure mapping of the 3′-terminal 166 nt of the MHV-JHM genome. We selected the 3′-terminal 166 nt for secondary-structure mapping by limited RNase digestion because this region contains two host protein binding elements identified by our laboratory. M*fold*, version 3.0, was used to generate thermodynamically stable secondary structures, and of the three models generated, the model which best fits our experimental data (see below) is shown (Fig. 1). Examination of secondary structures for possible pseudoknots was performed using software developed by Rivas and Eddy (25). None were predicted. To generate a homogenous RNA template, plasmid LITMUS 38 was chosen as the vector. LITMUS 38 contains an *Spe*I site at position 2460 within the T7 promoter, which we exploited for our cloning procedure. This allows transcription to initiate with the G at position 166. There are two T7 promoters (positions 2448 and 2773) within LITMUS 38; we originally planned to inactivate the downstream T7 promoter after cloning. However, a deletion during cloning destroyed the downstream T7 promoter. The recombinant LITMUS 38 was then linearized with *Mlu*I, gel purified, and used as a template for in vitro transcription. RNA transcripts were purified as described in Materials and Methods.

To probe the secondary structure of 166 + 11A RNA, sin-

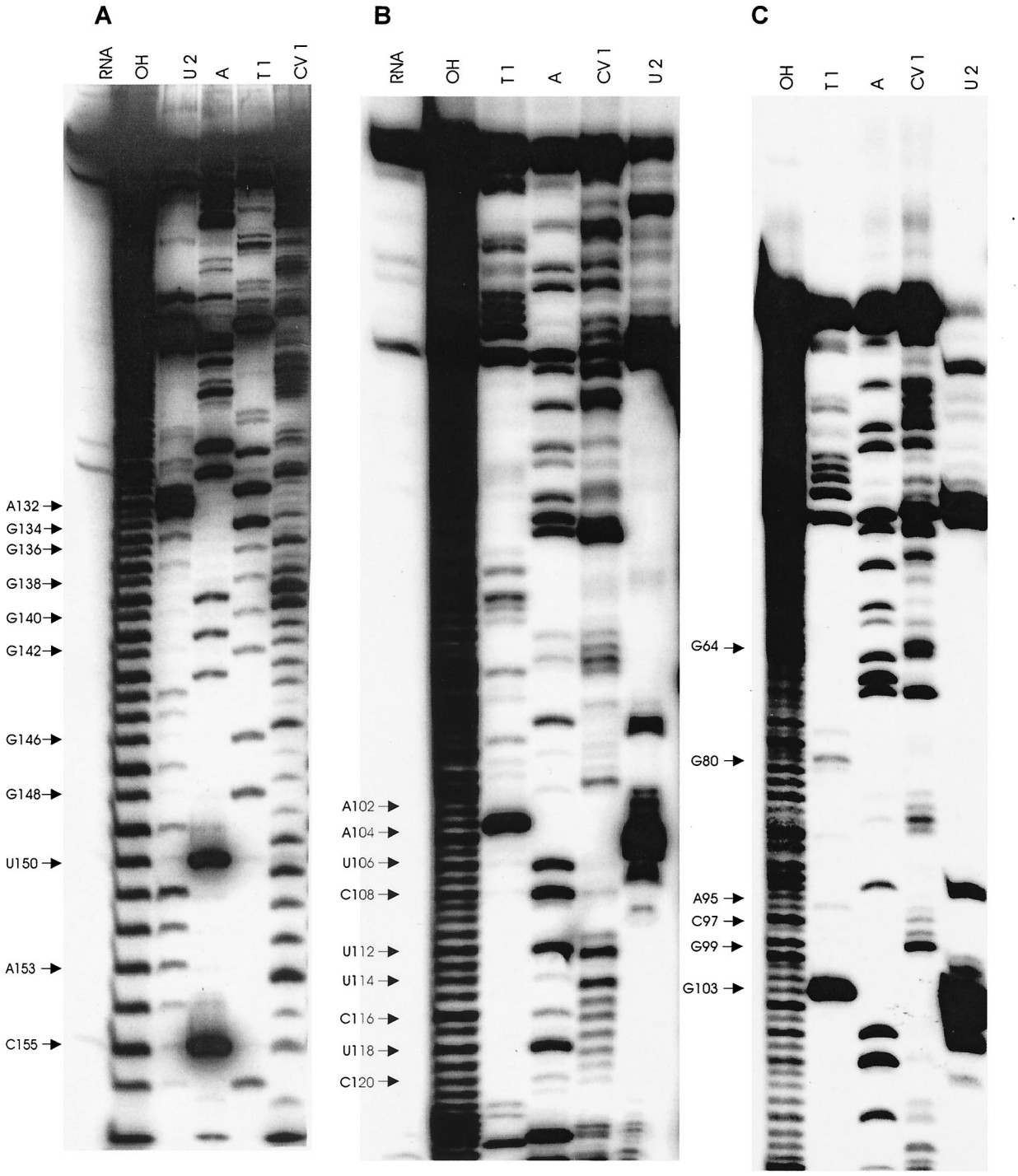

FIG. 2. Enzymatic probing of the 3′-terminal 166 + 11A RNA. Dephosphorylated, 5′-end-labeled, and gel-purified 166 + 11A RNA was subjected to limited digestion with RNase T_1 (0.0002 U), A (0.0002 U), U2 (2 U), and CV1 (0.07 U) on ice for 30 min. The digested products were resolved by electrophoresis in 7 M urea–20% polyacrylamide gels (A) or 7 M urea–10% polyacrylamide gels (B) for 4 h. Six hours of 7 M urea–10% PAGE was also employed (C) to enlarge the readable region. Lanes RNA (panels A and B), undigested 166 + 11A RNA; lanes OH, RNA ladders generated by limited alkaline hydrolysis of 166 + 11A RNA.

gle-strand-specific RNases T_1 (G specific), A (U and C specific), and U2 (A specific) and double-strand-specific RNase CV1 were employed. Digestion products were electrophoresed for 4, 6, and 8 h in 10% and 20% polyacrylamide gels in order to obtain the maximum structural information possible for the 166 + 11A RNA (Fig. 2). By combining data from analyses performed under various electrophoretic conditions, we were able to determine the structural conformation for approxi-

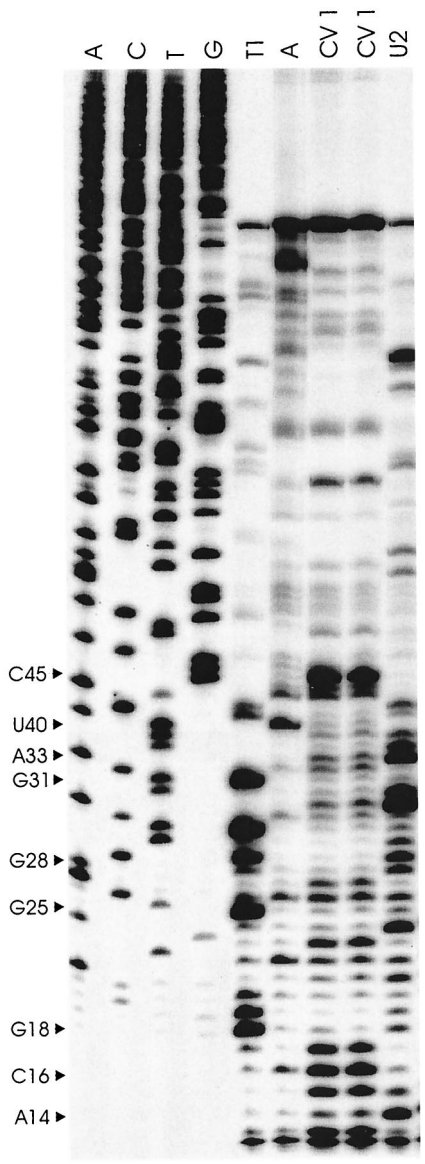

FIG. 3. Primer extension mapping of the secondary structure of the 3′-most 44 nt. Primer extension reactions with 5′-end-labeled oligonucleotide 5638B (Table 1) were performed with 166 + 11A RNA which had been subjected to limited digestion with single- and double-strand-specific RNases as described in Materials and Methods. Primer extension reaction products and DNA sequencing reaction products were loaded on the same gel to locate the primer extension products.

mately 114 nt spanning nt 157 to 44 upstream of the 3′ terminus of the MHV-JHM genome.

Primer extension of RNAs which had been subjected to limited RNase digestion was utilized to obtain data for the 3′-terminal 44 nt. To acquire the maximal structural information, we first established the minimum primer length needed to probe the 166 + 11A RNA structure. Our data show that an 18-nt primer containing 11 Ts plus the 3′-most 7 nt of 166-nt cDNA is the smallest primer that anneals to the RNA template (data not shown). The results from repeated primer extension experiments generated structural information encompassing positions 46 to 13 (Fig. 3). The positions of primer extension products were determined by loading a dideoxy sequencing ladder on the same gel. We were unable to obtain structural information for the 5′- and 3′-terminal 9 and 12 nt, respectively. Our secondary structure mapping data are summarized in Fig. 1 and indicated that multiple stem-loop and hairpin-loop structures exist in 166 + 11A RNA.

A 23-nt stem-loop structure within the nt 166 to 129 host protein binding element of MHV-JHM is conserved. Enzymatic probing, secondary structure modeling by M*fold*, and phylogenetic comparison between group II coronaviruses MHV and BCoV revealed a stem-loop structure common to both viruses. This stem-loop is composed of 23 nt in two separate strings which share conserved primary sequences (MHV, nt 142 to 132 and 68 to 79; BCoV, nt 130 to 120 and 65 to 76) and which have identical predicted secondary structures (Fig. 4). Within the conserved 23 nt, the formation of a 7-bp structure made up of nt 142 to 136 and 68 to 74 of the MHV genome was suggested by our RNase digestion experiments (142:68, G:U; 141:69, U:A; 140:70, G:C; 139:71, U:A; 138:72, G:C; 137:73, A:U; 136:74, G:C). Figure 2A shows that RNase CV1 digested the upstream side of this region (nt 142 to 136), producing multiple digestion products on a 20% denaturing gel. In particular, RNase CV1 digestion generated strong signals at G140, U139, G138, and A137. RNase A and RNase T_1 digestions gave weak signals at G142, U141, G140, U139, and G136, possibly due to the "breathing" of the stem. The digestion signals from the downstream nucleotides involved in the 7-bp configuration were more complicated. U68, A69, U73, and C74 were only cut by RNase CV1. C70 was cut weakly by RNase CV1 but strongly by RNase A. A71 did not give any structural information on the denaturing gel. C72 was cut by RNase CV1 and RNase A (Fig. 1). Overall the digestion patterns indicated that a 7-bp structure exists in this region. In addition, enzymatic probing revealed the presence of a loop structure involving nt 135 to 131 and nt 75 to 80 of MHV, immediately adjacent to the 7 nt stem described above. Nucleotides G131 and G134 were strongly cut by RNase T_1, whereas A132 and A133 were strongly digested by RNase U2. A135 was cut by both RNase U2 and CV1 (Fig. 2A). In the downstream side of the loop, nucleotides G80, A79, A78, G77, and G75 were weakly digested by single-strand-specific RNases (Fig. 2C).

Further support for the presence of the 23-nt stem-loop structure comes from computer modeling. The M*fold* prediction of the 166 + 11 RNA secondary structure generates three

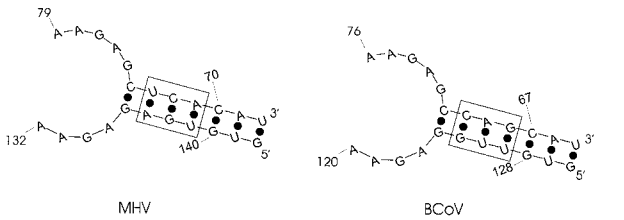

FIG. 4. A 23-nt stem-loop in 3′-terminal 166-nt genomic RNA is conserved in both MHV and BCoV. The primary sequences of nt 142 to 132 and 68 to 79 of MHV and nt 130 to 120 and 65 to 76 of BCoV are conserved with the exception of the boxed 6 nt, which covary to maintain identical secondary structures.

stable structures with minor variations in their d*G* values (d*G* = 31 ± 2 kcal/mol). All three models contain the conserved 23-nt stem-loop involving nt 142 to 132 and 68 to 79. The conservation of this 23-nt stem-loop structure is assisted by a phylogenetic comparison of MHV and BCoV predicted secondary structures. The M*fold* prediction of the 3′-terminal 166-nt RNA secondary structure of BCoV generates four thermodynamically stable secondary structures (d*G* = −38 ± 2 kcal/mol). All four models contain the 23-nt stem-loop structure at positions 130 to 120 and 65 to 76. The 7- nt stem structure spans nt 130 to 124 and pairs with nt 65 to 71 (130:65, G:U; 129:66, U:A; 128:67, G:C; 127:68, U:G; 126:69, U:A; 125:70, G:C; 124:71, G:C). Sequence comparison of the upstream side of the 7-nt stem structure between MHV (positions 142 to 136) and BCoV (positions 130 to 124) indicated the pattern as 5′-GUGUXYG-3′. Five out of seven residues are identical. In addition, nucleotide covariation is found within this 7-bp structure between MHV (139:71, U:A; 138:72, G:C; 137:73, A:U) and BCoV (127:68, U:G; 126:69, U:A; 125:70, G:C) (Fig. 4) in order to form the 7-nt stem structure. The loop region of the 23-nt conserved structure has an identical primary structure in MHV (positions 132 to 135 and 79 to 75) and in BCoV (positions 120 to 123 and 76 to 72) (Fig. 4).

When the data are compiled, it is clear that the 23-nt structural element is present in both MHV and BCoV despite slight position differences and minor primary sequence diversity. It is interesting that the upstream side (nt 142 to 132) of this 23-nt stem-loop structure of MHV is located in the upstream host protein binding element (nt 166 to 129) identified in our laboratory (21) and overlaps with the 11-nt conserved motif located at nt 139 to 129 (36).

Two hairpin-loop structures have been identified within the 3′ 166 + 11A RNA. A hairpin-loop structure spanning nt 116 to 96 was characterized in our experimental system. Seven continuous RNase CV1-digested products encompassing positions 119 to 113 were detected in Fig. 2B. Another five residues cleaved by RNase CV1 mapped to nt 99 to 95 (Fig. 2C). Combining the RNase digestion data and M*fold* modeling, we believe that a 4-bp stem exists at positions 116 to 113 and 96 to 99 in the 166 + 11A RNA under our conditions (116:96, C:G; 115:97, G:C; 114:98, U:G; 113:99, C:G). The existence of a loop structure from nt 110 to 100 was also detected by our limited RNase digestion assays. Single-strand-specific RNases strongly digested nucleotides C108, A107, U106, A105, A104, G103, and A102. Nucleotides A110, C109, A101, and C100 were weakly cut by single-strand-specific enzymes (Fig. 2B). However, enzymatic data for nucleotides U112 and A111 were not as distinct as those for their neighbors. U112 was cut weakly by both single-strand- and double-strand-specific enzymes, and A111 was cut weakly with a double-strand-specific nuclease. The data at these two positions do not exclude the possibility that the stem-loop structure forms but do suggest that an alternative structure may also form.

The M*fold* model (Fig. 1) predicts a much longer stem structure, nt 123 to 113 paired with nt 87 to 99, with two single-nucleotide bugles (at positions 90 and 95). A discrepancy between our enzymatic data and the predicted structural model arose at nt 122 to 123 and nt 93 to 94. According to the results from RNase digestion assays, G123 and G122 were weakly cut by RNase T_1. U94 and A93 were partially digested by RNase A and U2, respectively. Little digestion signal between nt C90, C88, and C87 was observed (Fig. 2C). Since the digestion data were generated by repeating experiments at least three times and were reproducible, we feel it is likely that a longer stem structure predicted by M*fold* was not stable or does not exist under our conditions.

Nucleotides 67 to 52 are predicted to form a hairpin-loop. This hairpin-loop is supported by observation that residues A66, G65, G64, G63, C54, U53, and G52 are digested only by RNase CV1 and not by single-strand-specific RNases U2, T_1, and A (Fig. 1). The included loop structure at position 62 to 57 was suggested by enzymatic data and M*fold* prediction. Nucleotides U62 and U59 were both strongly digested by single-strand-specific RNase A.

The identification of these two hairpin-loop structures, particularly the hairpin-loop structure at positions 67 to 52, has enabled us to eliminate the existence of one of the three predicted thermodynamically stable secondary structure models of the 166 + 11A RNA generated by M*fold*. The alternate model (not shown) differed only slightly from the model shown in Fig. 1 but was not as good a match with the enzymatic probing data.

Base pairing within the nt 142 to 68 region is required for efficient MHV DI RNA replication. Mutant DI RNAs were constructed to conduct a series of DI RNA replication assays to examine the role of RNA secondary structure within the 3′-terminal 166 nt of the MHV-JHM genome in replication. To test if structural elements identified by enzymatic probing exist in the context of a larger RNA molecule and to explore their biological functions, three stem structures were selected for mutagenesis to assess their role in replication. The putative structures we examined are stem A, a 7-nt stem with nt 142 to 136 paired with nt 68 to 74; stem B, part of a bulged stem-loop structure with nt 116 to 113 paired with 96 to 99; and stem C, part of a hairpin-loop structure with nt 67 to 63 paired with 52 to 56. Both sides of stems A and B were mutated to destroy the predicted base pairing. Mutant A1 contains four clustered transversions at positions 140 to 137, while mutant A2 also contains four transversions at positions 70 to 73. M*fold* predicts that, when the mutations introduced in A1 and A2 are coupled (mutant A12), the wild-type secondary structure is restored. Mutant B1 contains four transversions at positions 96 to 99; mutant B2 contains four transversions at positions 116 to 113. Mutant B12 was designed to have an effect similar to that, in terms of secondary structure, of mutant A12. Five transversions spanning nt 67 to 63 were introduced into stem C. To assure that we introduced only the desired mutations into plasmid DE25, a DE25 deletion mutant (see Materials and Methods) was constructed and utilized as a template in mutagenesis. After sequencing the 330-bp *Nru-Xba*I segment containing the introduced mutations, we transferred the introduced mutations into wild-type DE25 by restriction fragment exchange.

To determine the effects of the mutations predicted to disrupt secondary structure, wild-type and mutant DI RNAs were transfected into MHV-JHM-infected 17Cl-1 cells. After metabolic labeling with [^{32}P]orthophosphate, total intracellular RNA was extracted and analyzed by gel electrophoresis. The replication efficiency of each mutant relative to that of wild-type DE25 was measured with a Phosphorimager. As shown in

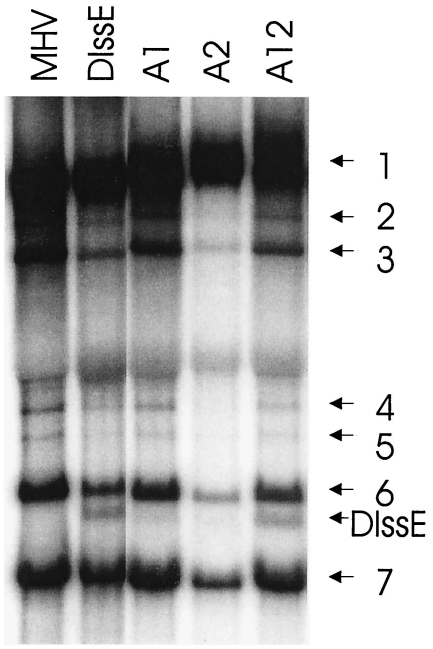

FIG. 5. Replication of wild-type DE25, mutants A1 and A2, and complementary mutant A12. 17Cl-1 cells were infected with MHV-JHM and transfected with DI RNAs 1 h later. Cells were labeled with [^{32}P]orthophosphate in the presence of actinomycin D when 20% of the cells had formed syncytia. Total RNA was isolated when syncytia involved 80% of the culture. RNAs (5 μg) were resolved in a formaldehyde–1% agarose gel at 110 V for 6 h. Arrows, positions of viral RNA1 to RNA7 and DI RNA.

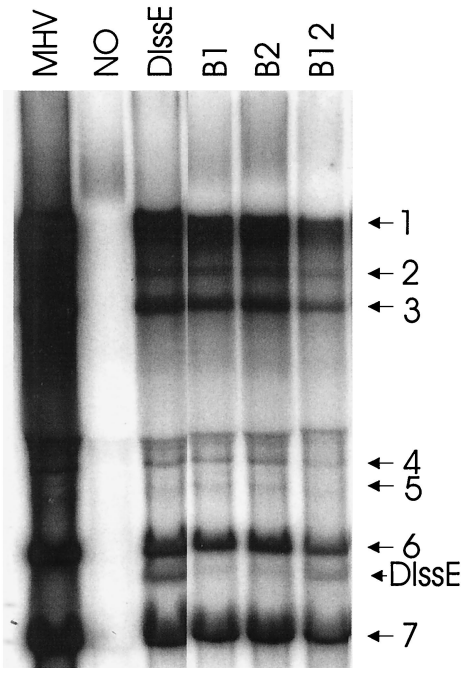

FIG. 6. Replication of wild-type DE25, mutants B1 and B2, and complementary mutant B12. Replication assays were performed as described for Fig. 5. Arrows, positions of viral RNAs and DI RNA.

Fig. 5 and Table 2, DI RNAs carrying the A1 and A2 mutations replicated only 17 and 30%, respectively, as well as DIssE. The overall amount of label incorporated into all MHV-specific RNAs in the culture transfected with the DI RNA carrying the A2 mutant was decreased in this experiment. This finding was not reproducible. This effect was taken into account by normalizing the data relative to RNA7 (Table 2). To distinguish the effect of the primary sequence from that of the secondary structure, complementary mutants were constructed in stem A (mutant A12). A DI RNA carrying the A12 mutation (restores stem A) replicated 92% as well as wild-type DI RNA. DI RNAs with mutations in stem B exhibited various decreases in their replication efficiencies (Fig. 6 and Table 2). The effect of mutation B1 (26%) was much more severe than that of mutation B2 (51%). When both mutations were introduced into DE25 to construct DI RNA B12 to maintain stem B, the DI replicon replicated at nearly wild-type levels (79%). Stem C mutations had only a minimal effect on DI replication (90%).

TABLE 2. Replication efficiency of each DI RNA mutant relative to that of wild-type DI RNA (DIssE)

Expt no.	Replication efficiency (%) of wild-type DIssE:						
	A1	A2	A12	B1	B2	B12	C
1	39.65 (R)[a]	—[b]	—	—	42.11	—	98.69
2	35.08 (R)	—	—	—	66.53	—	86.27
3	15.21	—	—	—	44.83	—	84
4	—	35.36	131.96	23.02	—	96.58	—
5	—	45 (R)	74	30	—	83	—
6	17	25	80	32	60 (R)	66	—
7	19	30	82	20	50	70	93
Avg[c]	17.07	30.12	91.99	26.25	50.87	78.90	90.49

[a] Numbers followed by (R) indicate that RT-PCR demonstrated the replicating DI RNA to be a wild-type recombinant.
[b] —, not done.
[c] Experiments in which recombination occurred were excluded in calculating mean replication efficiency.

The accurate detection of mutant DI RNA replication was complicated by occasional restoration of the wild-type sequence as a consequence of recombination between DI RNA and helper virus RNA. RT-PCR and sequencing of negative-strand RNA were carried out in every DI RNA replication assay to monitor recombination events. To eliminate detection of carryover transcription template DNA, 5 μg of total RNA was treated with 10 U of RNase-free DNase. PCR was performed prior to RT to assure that any remnant DNA was undetectable under our conditions, as described in Materials and Methods. Sequencing of RT-PCR products demonstrated that conversion of transfected DI RNA to the wild-type sequence occurred on a few occasions with single mutant DI RNAs A1, A2, and B1. No recombination was detected in assays for the complementary DI RNA mutants A12 and B12 (Table 2), implying that the restoration of secondary structure compensated for the severe effect on replication caused by our introduced structural changes.

DISCUSSION

We previously reported two host protein binding elements within the 3′-terminal 166 nt of the MHV genome (21, 36). In the present study, we probed the secondary structure of the 166 + 11A fragment; our findings show for the first time that

conserved secondary structure elements in this region function in DI RNA replication.

Conserved structural elements within the 3′ UTR of MHV and BCoV genomic RNA participate in DI RNA replication. Williams et al. identified a 54-nt hairpin type pseudoknot between nt 226 and 173 within the 3′ UTR and demonstrated that the pseudoknot was required for BCoV DI replication (34). Phylogenetic analysis indicated similar pseudoknot structures in other coronaviruses including MHV (34). Hsue et al. demonstrated a 68-nt multiple stem-loop structure spanning nt 302 to 234 within the 3′ UTR of MHV (7, 8). A similar structure also exists in BCoV. Functional studies suggested that three stems in this structure are essential for viral replication (7, 9). Our biochemical data revealed a 23-nt stem-loop structure in which nt 142 to 132 partially paired with nt 68 to 79 in the MHV genome. A phylogenetic comparison of MHV and BCoV as well as computer modeling revealed the existence of a homologous structure in BCoV at positions 130 to 120 and 65 to 76. MHV DI RNA replication assays demonstrated that this 7-bp structure was required for efficient DI RNA replication. We recognize that the 23-nt conserved structures exist in slightly different primary sequence positions in MHV and BCoV. However, an alignment between MHV and BCoV confirms that these are homologous sequences and have corresponding secondary structures. Inspection of the predicted secondary structures of the last 166 nt of BCoV (not shown) and MHV (Fig. 1) indicate that this is the only predicted secondary structure which is common to both viruses. It is of interest that octanucleotide motif GGAAGAGC (nt 81 to 74 of MHV; Fig. 1), which is the only sequence element in the 3′UTR which is conserved among all coronaviruses (groups I, II, III) entirely overlaps one side of this conserved internal loop in MHV (Fig. 1 and 4). Hsue's data (7, 9), Williams's data (34), and the data presented here show that structural elements within the 3′ UTRs of MHV and BCoV form important *cis*-acting signals that regulate viral replication. Conservation of structural elements could explain why the 3′ UTRs of MHV and BCoV are fully interchangeable, even considering the divergence of sequences within the 3′ UTRs, except for the highly conserved 3′-terminal 42 nt (8).

The discovery of an upstream 23-nt conserved stem-loop (nt 142 to 132) located in the upstream host protein binding element (nt 166 to 129) that also overlaps the 11-nt host binding motif (nt 139 to 129) identified by our laboratory (21, 37) may facilitate the characterization of *trans*-acting factors interacting with the upstream host protein binding element. So far, four host proteins with apparent molecular masses of 120, 55, 40, and 25 kDa are known to bind to this region (21). The identities of these proteins are still under investigation. Recently, heterogeneous nuclear ribonucleoprotein A1 (hnRNP A1) was found to bind strongly at positions 170 to 90 within the MHV 3′ UTR (10). Mutagenesis studies of this region showed hnRNP A1-RNA interaction was reduced when nucleotides at positions 131 to 135 were deleted or substituted. Nucleotides 131 to 135 are predicted by both M*fold*, version 3.0, and MulFold2 to be single stranded, which supports our digestion data; these nucleotides also fall within our conserved 23-nt stem-loop structure. Mutations at positions 131 to 135 also reduced RNA transcription and replication activity, suggesting a role for hnRNP A1 binding in the MHV life cycle (10). However, the role of hnRNP A1 binding to MHV sequences in vivo is controversial; Shen and Masters used a cell line that does not express hnRNP A1, CB3, to test the role of hnRNP A1 binding in replication (27). CB3 was able to efficiently grow MHV-A59 to wild-type titers, and correction of this defect did not alter MHV replication.

Several lines of evidence demonstrate that RNA secondary structures are involved in viral life cycles (4). Two stem-loop structures within the 3′ end of hepatitis E virus genomic RNA have been identified as possible *cis*-acting signals for binding to viral RNA-dependent RNA polymerase (RdRp). Mutations that destroy the stem-loop structure greatly reduce RdRp binding (1). The functional roles of human immunodeficiency virus (HIV) structural elements have also been investigated extensively. The conserved stem-loop structures in HIV type 1 (HIV-1) RNA regulate RNA splicing and mRNA translation (24). The functions of conserved secondary structures in plant viruses have also been studied (3, 13, 30, 35). The structural elements in the 3′ UTR of the barley yellow dwarf virus genome are required for cap-independent translation and communication with the 5′ end of the mRNA (6).

RNA molecules exist as thermodynamic populations. This characteristic of RNA molecules may cause a particular nucleotide to form different configurations, resulting in RNA molecules that are cut by both single-strand-specific and double-strand-specific RNases at the same time, as exhibited in our data. We also realize that some contradictory conformations were obtained by comparing our biochemical data and M*fold* predictions; i.e., A15, C16, and C17 were strongly cut by RNase CV1 in our limited digestion experiments. However, the same 3 nt are predicted to be in a loop structure by computer-assisted modeling. The most likely explanation is that the computer prediction is inaccurate at those positions, but we cannot eliminate the possibility that these 3 nt are located in a stacked single-stranded region or form tertiary structures with other nucleotides. The accessibility of each base to RNases also affects the limited RNase digestion signals. If some nucleotides are protected by other nucleotides three dimensionally, they will not be cut by an RNase, resulting in no digestion signal and lack of structural information for those nucleotides. Our data have demonstrated this possibility; i.e., nucleotides C87 and C88 gave no digestion signal although adjacent nucleotides gave distinct signals.

Considerable progress in identifying *cis*-acting sequences within the 3′ UTR has been made. Secondary structures of *cis*-acting sequences provide targets for mutagenesis to determine their role in MHV replication. They may also provide binding sites for *trans*-acting factors, which may participate in the MHV life cycle. To date we have identified the four proteins binding to the 3′(+)42 protein binding element as mitochondrial aconitase (23), mitochondrial HSP70 (S. K. Nanda and J. L. Leibowitz, submitted for publication), and HSP60 and HSP40 (Nanda and Leibowitz, submitted). Based on UV cross-linking assays with the host protein binding element at nt 166 to 129 and the 3′(+)42 host protein-binding element, it is possible that some of the proteins that bind to the 3′(+)42 host protein binding element and the protein binding element at nt 166 to 129 are identical. Work continues to identify the host proteins and the role of their binding elements in MHV genome replication.

ACKNOWLEDGMENTS

This work was supported by in part by National Multiple Sclerosis Society grant RG2203-B-6 and a generous gift from the Stearman family.

We thank Santosh K. Nanda, Elena Belyavskaya, and Laura Owen for help and encouragement and Judy Ball for thoughtful reading of the manuscript.

REFERENCES

1. **Agrawal, S., D. Gupta, and S. K. Panda.** 2001. The 3′ end of hepatitis E virus (HEV) genome binds specifically to the viral RNA-dependent RNA polymerase (RdRp). Virology **282:**87–101.
2. **Barthold, S. W.** 1987. Host age and genotypic effects on enterotropic mouse hepatitis virus infection. Lab. Anim. Sci. **37:**36–40.
3. **Bernal, J. J., and F. Garcia-Arenal.** 1997. Analysis of the in vitro secondary structure of cucumber mosaic virus satellite RNA. RNA **3:**1052–1067.
4. **Chen, D., M. Barros, E. Spencer, and J. T. Patton.** 2001. Features of the 3′-consensus sequence of rotavirus mRNAs critical to minus strand synthesis. Virology **282:**221–229.
5. **DeGroot, R. J., R. G. van der Most, and W. J. M. Spaan.** 1992. The fitness of defective interfering murine coronavirus DI-a and its derivatives is decreased by nonsense and frameshift mutations. J. Virol. **66:**5898–5905.
6. **Guo, L., E. Allen, and W. A. Miller.** 2000. Structure and function of a cap-independent translation element that functions in either the 3′ or the 5′ untranslated region. RNA **6:**1808–1820.
7. **Hsue, B., T. Hartshorne, and P. S. Masters.** 2000. Characterization of an essential RNA secondary structure in the 3′ untranslated region of the murine coronavirus genome. J. Virol. **74:**6911–6921.
8. **Hsue, B., and P. S. Masters.** 1997. A bulged stem-loop structure in the 3′ untranslated region of the genome of the coronavirus mouse hepatitis virus is essential for replication. J. Virol. **71:**7567–7578.
9. **Hsue, B., and P. S. Masters.** 1998. An essential secondary structure in the 3′ untranslated region of the mouse hepatitis virus genome. Adv. Exp. Med. Biol. **440:**297–302.
10. **Huang, P., and M. M. Lai.** 2001. Heterogeneous nuclear ribonucleoprotein a1 binds to the 3′-untranslated region and mediates potential 5′-3′-end cross talks of mouse hepatitis virus RNA. J. Virol. **75:**5009–5017.
11. **Kim, Y., and S. Makino.** 1995. Characterization of a murine coronavirus defective interfering RNA internal *cis*-acting replication signal. J. Virol. **69:**4963–4971.
12. **Kim, Y.-N., Y. S. Jeong, and S. Makino.** 1993. Analysis of cis-acting sequences essential for coronavirus defective interfering RNA replication. Virology **197:**53–63.
13. **Kwon, C. S., and W. Chung.** 1999. A single-stranded loop in the 5′ untranslated region of cucumber mosaic virus RNA 4 contributes to competitive translational activity. FEBS Lett. **462:**161–166.
14. **Lai, M. M. C., R. S. Baric, P. R. Brayton, and S. A. Stohlman.** 1984. Characterization of leader RNA sequences on the virion and mRNAs of mouse hepatitis virus, a cytoplasmic RNA virus. Proc. Natl. Acad. Sci. USA **81:**3626–3630.
15. **Lai, M. M. C., P. R. Brayton, R. C. Armen, C. D. Patton, C. Pugh, and S. A. Stohlman.** 1981. Coronavirus: a jumping RNA transcription. J. Virol. **39:** 823–834.
16. **Lai, M. M. C., and S. A. Stohlman.** 1978. The RNA of mouse hepatitis virus. J. Virol. **26:**236–242.
17. **Lampert, P. W., J. K. Sims, and A. J. Kniazeff.** 1973. Mechanism of demyelination in JHM encephalomyelitis. Electron microscopic studies. Acta Neuropathol. **24:**76–85.
18. **Leibowitz, J. L., K. C. Wilhelmsen, and C. W. Bond.** 1981. The virus-specific intracellular RNA species of two murine coronaviruses: MHV-A59 and MHV-JHM. Virology. **114:**39–51.
19. **Lin, Y.-J., and M. M. C. Lai.** 1993. Deletion mapping of a mouse hepatitis virus defective interfering RNA reveals the requirement of an internal and discontinuous sequence for replication. J. Virol. **67:**6110–6118.
20. **Lin, Y.-J., C.-L. Liao, and M. M. C. Lai.** 1994. Identification of the *cis*-acting signal for minus-strand RNA synthesis of a murine coronavirus: implications for the role of minus-strand RNA in RNA replication and transcription. J. Virol. **68:**8131–8140.
21. **Liu, Q., W. Yu, and J. L. Leibowitz.** 1997. A specific host cellular protein binding element near the 3′ end of mouse hepatitis virus genomic RNA. Virology **232:**74–85.
22. **Makino, S., C.-K. Shieh, L. H. Soe, S. C. Baker, and M. M. C. Lai.** 1988. Primary structure and translation of a defective interfering RNA of murine coronavirus. Virology **166**.
23. **Nanda, S. K., and J. L. Leibowitz.** 2001. Mitochondrial aconitase binds to the 3′ untranslated region of the mouse hepatitis virus genome. J. Virol. **75:** 3352–3362.
24. **Rhim, H., and A. P. Rice.** 1994. Functional significance of the dinucleotide bulge in stem-loop1 and stem-loop2 of HIV-2 TAR RNA. Virology **202:**202–211.
25. **Rivas, E., and S. R. Eddy.** 1999. A dynamic programming algorithm for RNA structure prediction including pseudoknots. J. Mol. Biol. **285:**2053–2068.
26. **Robb, J. A., and C. W. Bond.** 1979. Coronaviridae, p. 193–247. *In* H. Fraenkel-Conrat and R. R. Wagner (ed.), Comprehensive virology, vol. 14. Plenum Press, New York, N.Y.
27. **Shen, X., and P. S. Masters.** 2001. Evaluation of the role of heterogeneous nuclear ribonucleoprotein A1 as a host factor in murine coronavirus discontinuous transcription and genome replication. Proc. Natl. Acad. Sci. USA **98:**2717–2722.
28. **Spaan, W., H. Delius, M. A. Skinner, J. Armstrong, P. Rottier, S. Smeekens, S. G. Siddell, and B. A. M. van der Zeijst.** 1984. Transcription strategy of coronaviruses: fusion of noncontiguous sequences during mRNA synthesis. Adv. Exp. Biol. Med. **173:**173–186.
29. **Spaan, W. J. M., P. J. M. Rottier, M. C. Horzinek, and B. A. M. van der Zeijst.** 1981. Isolation and identification of virus-specific mRNAs in cells infected with mouse hepatitis virus. Virology **108:**424–434.
30. **Wang, J., and A. E. Simon.** 2000. 3′-end stem-loops of the subviral RNAs associated with turnip crinkle virus are involved in symptom modulation and coat protein binding. J. Virol. **74:**6528–6537.
31. **Wege, H., A. Muller, and V. ter Meulen.** 1978. Genomic RNA of the murine coronavirus JHM. J. Gen. Virol. **41:**217–227.
32. **Weiss, S. R., and J. L. Leibowitz.** 1981. Comparison of the RNAs of murine and human coronaviruses. Adv. Exp. Med. Biol. **142:**245–259.
33. **Wilhelmsen, K. C., J. L. Leibowitz, C. W. Bond, and J. A. Robb.** 1981. The replication of murine coronaviruses in enucleate cells. Virology **110:**225–230.
34. **Williams, G. D., R. Y. Chang, and D. A. Brian.** 1999. A phylogenetically conserved hairpin-type 3′ untranslated region pseudoknot functions in coronavirus RNA replication. J. Virol. **73:**8349–8355.
35. **Wu, B., W. B. Vanti, and K. A. White.** 2001. An RNA domain within the 5′ untranslated region of the tomato bushy stunt virus genome modulates viral RNA replication. J. Mol. Biol. **305:**741–756.
36. **Yu, W., and J. L. Leibowitz.** 1995. A conserved motif at the 3′ end of mouse hepatits virus genomic RNA required for host protein binding and viral RNA replication. Virology **214:**128–138.
37. **Yu, W., and J. L. Leibowitz.** 1995. Specific binding of host cellular proteins to multiple sites within the 3′ end of mouse hepatitis virus genomic RNA. J. Virol. **69:**2016–2023.